Meteoric smoke and meteor influx from global SOFIE observations

Mark E. Hervig[1], John M. C. Plane[2] , Dave E. Siskind[3], Wuhu Feng[2,4], Charles G. Bardeen[5], and Scott M. Bailey[6].

[1]GATS, Driggs, Idaho, USA.

[2]School of Chemistry, University of Leeds, Leeds, UK.

[3]Space Science Division, Naval Research Laboratory, Washington, DC, USA.

[4]NCAS School of Earth and Environment, University of Leeds, Leeds, UK.

[5]National Center for Atmospheric Research, Boulder, Colorado, USA.

[6]Virginia Polytechnic Institute, Blacksburg, Virginia, USA.

Corresponding author: Mark Hervig (m.e.hervig@gats-inc.com)

Main Points:

1) The composition of smoke in the mesosphere is consistent with iron-rich olivine.

2) Global ablated meteoric influx is 7.3 ± 2.0 t d^{-1}, with a total influx of 25.0 ± 7.0 t d^{-1}.

3) Smoke and H_2O are consistent with stronger winter descent in the Northern mesosphere relative to the South.

Abstract. Measurements from the Solar Occultation For Ice Experiment (SOFIE) are used to characterize meteoric smoke and meteor influx in both hemispheres. New smoke extinction retrievals from sunrise measurements in the Northern Hemisphere (NH) are presented, which complement the previously reported sunset observations in the Southern Hemisphere (SH). The sunrise observations are in good agreement with simulations from the Whole Atmosphere Community Climate Model (WACCM), for both the seasonal and height dependence of smoke in the mesosphere. The SOFIE - WACCM comparisons assumed that smoke in the mesosphere exists purely as Fe-rich olivine. This is justified because olivine is detected optically by SOFIE, it has the same elemental abundance as incoming meteoroids, and it is anticipated by theory and laboratory experiments. Treating mesospheric smoke as olivine furthermore brings closure in terms of the ablated and total meteoric influx determined here from SOFIE and a recent and independent investigation based on models and observations. SOFIE observations from 2007 - 2021 indicate a global ablated meteoric influx of 7.3 ± 2.0 metric tons per day (t d^{-1}), which corresponds to a total influx (ablated plus surviving material) of 25.0 ± 7.0 t d^{-1}. Finally, SOFIE indicates less smoke in the polar winter SH compared to NH winter. Finally, the results indicate stronger descent in the NH polar winter mesosphere than in the SH winter. This hemispheric asymmetry is indicated by smoke and water vapor results from both SOFIE and WACCM.

1. Introduction

A layer of meteoric smoke resides in the mesosphere and stratosphere, as nanometer sized aerosol that results from the ablation of cosmic dust particles during atmospheric entry [*Plane et al.*, 2012; *Hervig et al*., 2017a]. Smoke in the mesosphere is enhanced during polar winter and reduced in summer, due to transport by the global meridional mesospheric circulation. This behavior was first predicted by a two-dimensional model [*Megner et al*., 2008] and later observed by the Solar Occultation for Ice Experiment (SOFIE) [*Hervig et al.*, 2009]. The annual variation in smoke occurs despite the annual variation in meteoric influx (MI), which is highest (lowest) near the fall (spring) equinox [*Fentzke et al*., 2008]. The phase difference between smoke in the middle atmosphere and meteoric influx is due to the dominance of transport in the mesosphere, as discussed by *Bardeen et al.* [2008].

Estimates of the total meteoric influx (TMI, ablated plus surviving material) into Earth's atmosphere have ranged from 1 to 270 metric tons per day (t d^{-1}) [e.g., *Plane*, 2012]. The most recent results, however, appear to be converging on a narrower range (30 - 60 t d^{-1}) than previously. *Gardner et al.* [2014] report a TMI of 60 ± 16 t d^{-1} based on mid-latitude lidar observations of sodium near the mesopause combined with models. *Carrillo-Sánchez et al.* [2016] derived a TMI of 43 ± 14 t d^{-1} by combining a meteoric ablation model with a solar system dust model, constrained by lidar measurements of the vertical fluxes of mesospheric Na and Fe at mid-latitudes and cosmic spherule deposition at the South Pole. Importantly, they also found that only ~18% of the incoming meteoric material is ablated (and thus resident in the middle atmosphere), far lower than previous estimates (>80%). *Hervig et al.* [2017a] used SOFIE satellite observations of meteor smoke in the Southern Hemisphere (SH) mesosphere to derive a TMI of 30 ± 18 t d^{-1}. Most recently, *Carrillo-Sánchez et al.* [2020] report an update to the *Carrillo-Sánchez et al.* [2016] analysis (a new

chemical ablation model) which suggests TMI = 28 ± 16 t d^{-1}, and a slightly higher ablated fraction (30%) than previously.

The present study uses SOFIE observations to examine the time and height dependence of meteoric smoke in the Northern Hemisphere (NH), for the first time. This advance comes from new methods for calibrating the detector response drift during sunrise, which has been more challenging than for the sunset measurements. The new smoke results are compared to models and to SOFIE sunset observations, and subsequently used to determine meteoric influx during 2007 - 2021 in both hemispheres.

2. SOFIE Observations

SOFIE has observed temperature, five gases (O_3, H_2O, CO_2, CH_4, and NO), polar mesospheric clouds (PMC), and meteoric smoke, from the Aeronomy of Ice in the Mesosphere (AIM) satellite during 2007 - present [*Russell et al.*, 2009]. The occultation measurements are used to conduct retrievals at altitudes from roughly 20 to 95 km (up to 150 km for NO), with a vertical resolution of ~1.8 km. The measurement latitudes have evolved over the years, with dedicated polar coverage from 2007 – 2016 and 2019 – present. The years from 2017 - 2019 had equatorial coverage with some interruptions, and a change from sunsets (sunrise) in the SH (NH) to the NH (SH), due to progression of the AIM orbit (Figure 1). The current SOFIE data is version 1.3 which is available online (sofie.gats-inc.com).

The primary challenge in interpreting the meteoric smoke signals is accounting for a small drift in detector responsivity, which occurs due to heating of the system during solar view. The response drift is small (< 10 counts) compared to the dynamic range (2^{15} counts), but significant in terms of the response due to meteoric smoke (< 20 counts). For sunset observations the drift is highly linear, and is successfully removed by extrapolating a fit to measurements above the

atmosphere (exo-atmospheric) to lower heights [*Gordley et al.*, 2009]. Results for sunset smoke observations were first described by *Hervig et al.* [2009], who reported smoke extinction ($\beta(\lambda)$) at 1037 nm wavelength (λ). An updated response calibration approach [*Hervig et al.*, 2017a] provided sunset smoke extinctions at the additional wavelengths of 330 and 867 nm, which subsequently allowed the chemical composition of smoke to be identified. Sunset measurements benefit from a long period of solar observation above the atmosphere, which allows the instrument temperature to achieve a state of steady linear change, facilitating straightforward corrections to the signals. The drift in sunrise measurements is more difficult to characterize, however, because the atmosphere is observed before the instrument temperature has a chance to stabilize.

Figure 1. The latitude of SOFIE sunrise and sunset observations, from May 2007 through February 2021.

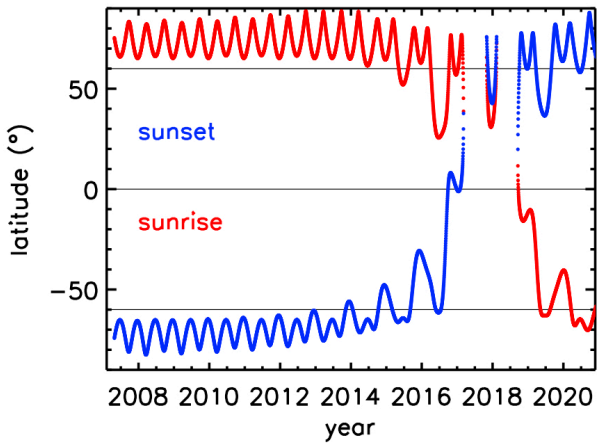

The drift in sunrise observations above the atmosphere was found to be consistent with a third order polynomial. Attempting such a high-order fit to individual measurements can be problematic, however, as variations due to noise can cause unrealistic values in the subsequent extrapolation to atmospheric altitudes. This issue is eliminated when fitting a polynomial to the average signal versus height based on multiple days (15 observations per day) as discussed in *Hervig et al.* [2017a]. The results here used 10-day averages (150 profiles), as shown in the example in Figure 2, where the response (R) minus the exo-atmospheric response (R_{EXO}) is shown

versus height. This approach was found to reduce the statistical uncertainty in the drift corrections to levels that were below both the statistical noise limit (~0.3 counts, see *Gordley et al.*, 2009) and the atmospheric response. The uncertainty in retrieved smoke extinction is defined as the root-sum-square of the measurement noise, drift correction uncertainty, and errors in removal of interference. Interference is due to O_3 absorption and Rayleigh scattering at 330 and 867 nm, and only Rayleigh at 1037 nm. As a result the 1037 nm observations have the lowest uncertainties, and are thus are used here to determine meteoric influx.

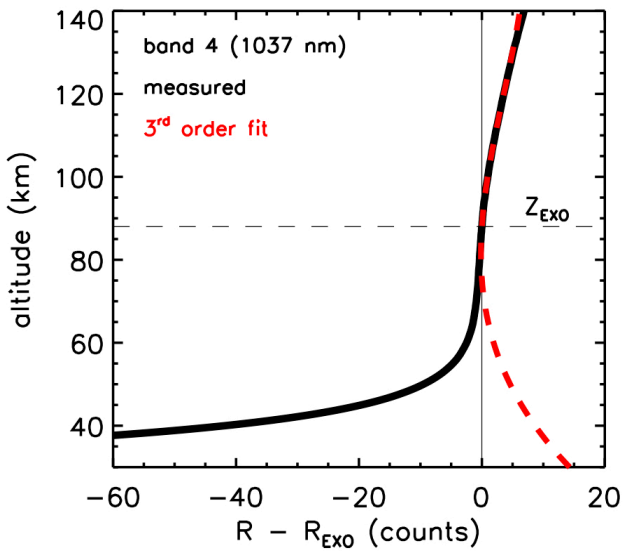

Figure 2. Example of SOFIE sunrise observations, as the response (R) minus that measured (R_{EXO}) at the exo-atmospheric height (Z_{EXO}). The profile is an average over 10 days (150 profiles) during December 1 - 10, 2010 (~70°N latitude). A third order polynomial fit at heights from Z_{EXO} to Z_{EXO} + 30 km is also shown. Note that the corrected response is the difference of the black and red curves.

For this work meteoric smoke extinctions were retrieved using 10-day averages of SOFIE signals, for observations from 2007 - 2021. The signal averages used only measurements that were free of PMCs, which are opaque enough to overwhelm the signal due to smoke. For the new sunrise (NH) observations reported here, this results in a lack of smoke extinctions during June and July when PMCs are ubiquitous at polar latitudes. Similarly, SH smoke extinctions are rarely obtained during December - January.

SOFIE measurements of smoke extinction are converted to volume density (V) using the relationship reported by *Hervig et al.* [2017a], $V = C\,\beta(1037)$, where C is a constant that varies with smoke composition. This linear relationship exists because at the SOFIE wavelengths smoke attenuation is entirely due to absorption, which is proportional to the particle radius cubed. Obtaining estimates of V from SOFIE allows direct comparison with the models, and also provides a means to determine meteoric influx. SOFIE multi-wavelength observations show that the most likely (>60% detection probability) smoke compositions are magnesiowüstite ($Mg_xFe_{1-x}O$, x = 0, 0.1, 0.2, and 0.6) and iron-rich olivine ($Mg_{0.8}Fe_{1.2}SiO_4$) [*Hervig et al.*, 2017a]. Note that values of C span roughly 250 to 1900 ($\mu m^3\ cm^{-3}$ km) for the potential smoke compositions. Furthermore, the different compounds are identified simultaneously, due to their spectral similarity combined with SOFIE uncertainties. Of the compounds indicated by SOFIE, only olivine has an elemental makeup that is similar to the relative elemental abundances of ablated meteoric material (see Table 1). Furthermore, laboratory and theoretical studies suggest that iron-rich olivine should result from the recombination of meteoric ablation products in the mesosphere [*Saunders and Plane*, 2011]. Taking these clues, the SOFIE extinctions were analyzed below assuming that smoke consists only of $Mg_{0.8}Fe_{1.2}SiO_4$. The first consequence is that the conversion of extinction to volume density becomes $V/\beta = 1512 \pm 1\ \mu m^3\ cm^{-3}$ km. This is in contrast to the previous interpretation which used the average V/β for the possible compositions ($687 \pm 470\ \mu m^3\ cm^{-3}$ km), and accepted the large standard deviation as an experimental uncertainty [*Hervig et al.*, 2017a]. Note that the resulting SOFIE V (and MI) are increased here by a factor of ~2 compared to previous results. The second consequence of assuming $Mg_{0.8}Fe_{1.2}SiO_4$ is that the SOFIE ablated influx has an elemental breakdown consistent with that predicted by combining chemical ablation and solar system dust models with observations [*Carrillo-Sánchez et al.,* 2020]. This in turn provides a straightforward

relationship between the ablated meteoric influx determined from SOFIE (see Section 5) and total meteoric influx (ablated plus surviving material).

Table 1. Relative abundance of the top five meteoric elements, for incoming meteoroids, and for the top three smoke compositions identified by SOFIE.

Element	Ablated Influx[1] ($t\ d^{-1}$)	Influx Fraction[1] (% by wt.)	Olivine[2] $Mg_{0.8}Fe_{1.2}SiO_4$ (% by wt.)	Magnesiowüstite[2] $Mg_{0.6}Fe_{0.4}O$ (% by wt.)	Wüstite[2] FeO (% by wt.)
Fe	2.8	34	38	42	78
O	2.7	32	36	30	22
Si	1.2	14	16	-	-
Mg	1.0	12	11	27	-
Na	0.3	3	-	-	-

[1]According to *Carrillo-Sanchez et al.* [2020].
[2]Identified using SOFIE smoke observations by *Hervig et al.* [2017a]. The detection probabilities were 68% for olivine, 75% for magnesiowüstite, and 71% for wüstite.

3. WACCM Model

This work used a model description of meteoric smoke based on a first principles representation in the Whole Atmosphere Community Climate Model (WACCM), as originally described by *Bardeen et al.* [2008]. The model begins with meteoric ablation products as metal-rich molecular clusters of 0.25 nm radius, and simulates the evolution of smoke particles due to growth by agglomeration, sedimentation, and transport. The model includes annual and latitudinal variations in meteoric influx [*Fentzke et al*., 2008], with the ablated meteoric influx (AMI) specified as the annual global mean. Note that the model only considers the ablated fraction of incoming meteoroids, since the surviving material falls quickly to the surface [*Plane et al.*, 2012]. Later model adaptations used the original smoke component of *Bardeen et al.* [2008] incorporated in the specified dynamics (SD) version of WACCM [*Bardeen et al.*, 2010]. The smoke simulations were later integrated into NCAR Community Earth System Model (CESM) version of WACCM [*Marsh et al.*, 2013a; 2013b], along with new descriptions of the gas-phase chemistry of meteoric metals and interactions between smoke and trace gases [*Plane et al.,* 2015; *Frankland et al.*, 2015;

James et al., 2017]. Finally, the model is nudged with the Modern-Era Retrospective Analysis for Research and Applications (MERRA2) [*Molod et al.*, 2015; *Gelaro et al.*, 2017]. This is the version used here, which is maintained at the University of Leeds, and was previously used in comparisons with SOFIE by *Hervig et al.* [2017a]. WACCM results for 2007 - 2020 were used here to determine daily zonal means which were sampled to the SOFIE latitude versus time.

4. Meteoric Smoke

The new SOFIE NH (sunrise) smoke V profiles are compared to SOFIE observations in the SH (sunset) in Figure 3a, where the results are averages for winter months when smoke is highest. The NH and SH observations are generally similar; however, note that SOFIE shows greater extinction in the NH middle mesosphere. Results from WACCM are also shown in Figure 3a, where SOFIE is systematically greater than WACCM in the lower mesosphere (P > ~0.5hPa). This difference was explored by *Hervig et al.* [2017b], who found that it was consistent with a layer of neutralized sulfate mixed with smoke at altitudes above the nominal sulfate layer during autumn - winter, when temperatures are low. SOFIE indicates a larger hemispheric (NH vs. SH) difference in the middle mesosphere (~0.2 - 0.01 hPa) than is shown by WACCM. These differences are further illustrated in Figure 3b, where the NH / SH V ratios are shown versus height. This rendition shows that SOFIE and WACCM both indicate a similar height dependence in the hemispheric difference, but that SOFIE differences (~65% at 0.1 hPa) are much larger than WACCM (~12% at 0.1 hPa). The seasonal variation in smoke is largely driven by the global mesospheric meridional circulation, where the polar winter maximum is due to transport of smoke from across the globe. The larger hemispheric differences indicated by SOFIE could thus be the result of a stronger circulation in the NH winter (or weaker in SH winter) than is contained in the model. Another possibility is seasonal variability in the global meteoric input function. However,

the variation that is currently in WACCM, which is based on the dust sources at 1 AU in the solar system, indicates a very symmetric annual-average distribution with respect to latitude and season [*Feng et al.*, 2013]. At pressures lower than ~0.01 hPa, SOFIE results are increasingly affected by noise, and the NH - SH differences at these heights are not taken seriously at this time.

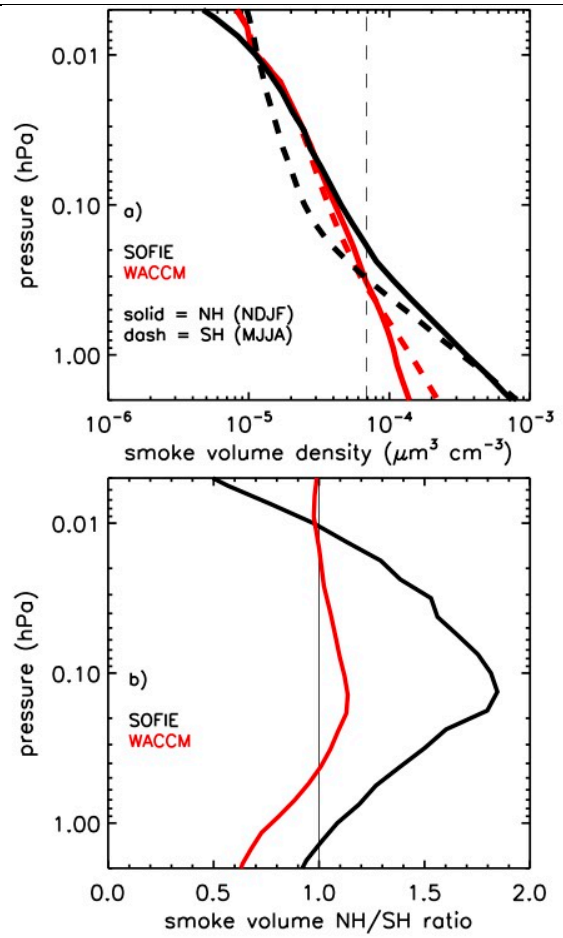

Figure 3. a) Meteor smoke volume density from SOFIE and WACCM, as averages during polar winter in the SH (~70°S, May - August) and NH (~70°N, November – February). The results are for 2007 - 2015 (before the SOFIE orbit change), when SOFIE NH (SH) measurements were from sunrises (sunsets) only (see Figure 1). The WACCM results were sampled to the SOFIE latitude vs. time. b) the ratio of NH / SH volume density from SOFIE and WACCM.

Time series of the new SOFIE sunrise (NH) smoke volume densities are compared to WACCM in Figure 4a, as the average V for 0.2 - 0.01 hPa (V′). The SOFIE - WACCM agreement is rather good, where both indicate similar annual variability and even a twin peak during winter. The exception is during winter 2013/14 where SOFIE V′ is greater than in WACCM (Figure 4a), a difference that is currently not understood. The seasonal variation in smoke is shown in greater

185 detail in Figure 4b, where the annual time series are based on averages including 2007 - 2013.
186 Recall that SOFIE smoke observations in summer are generally not useful due to contamination
187 by PMCs. The agreement is very good concerning the timing and depth of the annual smoke
188 variation, with the exception that WACCM shows a later start to the autumn - winter enhancement
189 than SOFIE. This difference is most likely due to different timing of the seasonal transition in
190 WACCM compared to the real atmosphere.

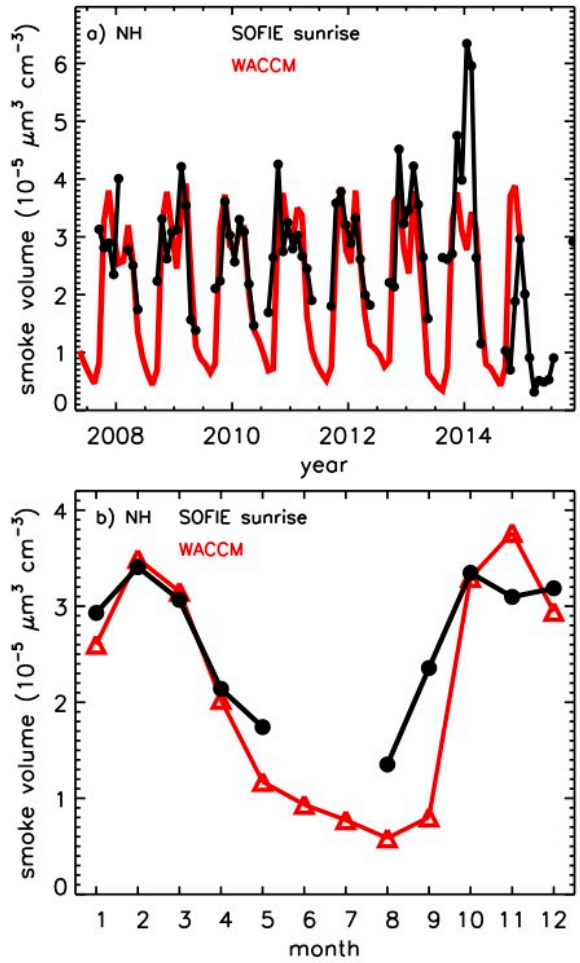

Figure 4. Time series of smoke volume density near 70°N latitude, for the vertical average of V over 0.2 to 0.01 hPa (V′). a) Time series of monthly zonal means from SOFIE and WACCM for 2007 - 2015 (before the SOFIE orbit changed). b) Annual time series as monthly zonal means for 2007 - 2013, from SOFIE and WACCM. The WACCM results were scaled to match SOFIE.

191

192 The year-to-year smoke variations were examined further using winter averages. The
193 latitude of SOFIE observations in winter was consistently near ~70° in both hemispheres, with the
194 exception of 2017 - 2018 when lower latitudes were sampled due to the changing AIM orbit

(Figure 5a). The comparison of smoke V′ (Figure 5b) highlights the hemispheric asymmetry indicated by SOFIE (NH > SH), that is also present (although weaker) in WACCM (e.g., Figure 3). The SOFIE NH observations show greater interannual variations than the SH measurements, which is consistent with greater variability in NH polar winter relative to the SH [*Schoeberl and Newman,* 2015]. WACCM also shows greater year-to-year variability in the NH compared to the SH, although variability in SOFIE is typically greater than in the model. Some of the interannual variability is due to the changing SOFIE latitudes after 2017, and this is captured in WACCM because the model was sampled to the SOFIE latitude vs. time. It is noteworthy, however, that SOFIE indicates more smoke in the NH not only during 2007 - 2018 when the NH was observed by sunrise occultations, but also in later years when the NH was observed by sunsets. This suggests that the hemispheric asymmetry is not due to a bias between the sunrise and sunset operational modes in SOFIE, but rather is a real characteristic of smoke in the mesosphere.

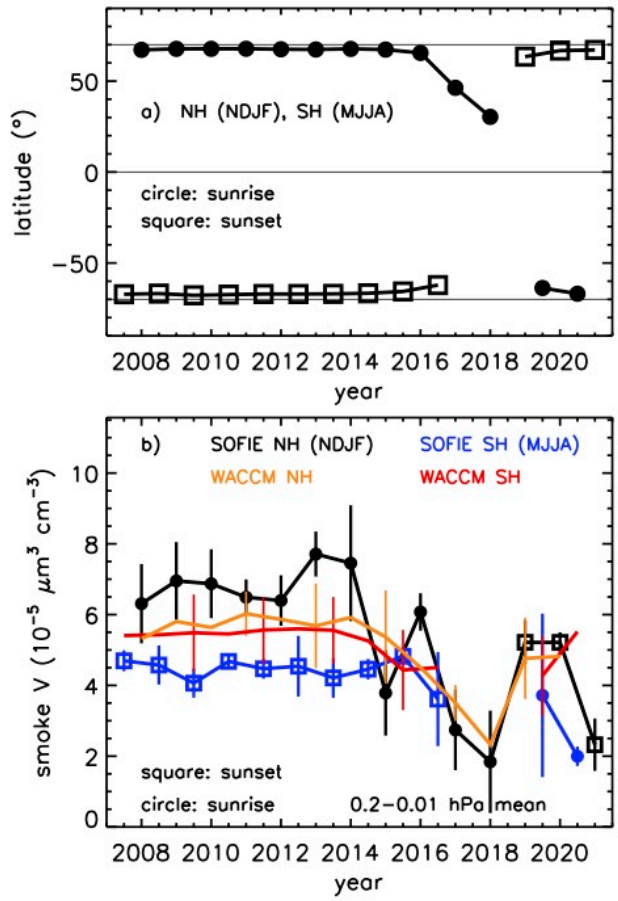

Figure 5. a) Time series of SOFIE measurement latitudes as winter means in the NH (November - February) and SH (May - August). b) The winter mean smoke volume density from SOFIE and WACCM, as the average for 0.2 to 0.01 hPa (V′). The results correspond to the latitudes in Figure 5a. Error bars indicate the standard deviation during each winter. WACCM results were scaled to match SOFIE.

The hemispheric difference in smoke was further explored by looking at water vapor in the upper mesosphere. Because H_2O behaves as a transport tracer and has a sharp vertical gradient in the mesosphere, it could indicate hemispheric differences that can confirm those in meteoric smoke. SOFIE and WACCM H_2O were examined as winter means in the upper mesosphere (0.2 - 0.01 hPa average, as for smoke). The results (Figure 6) show that there is less H_2O in the NH polar winter than in the SH polar winter, in both SOFIE and WACCM. *Lossow et al.* [2009] were the first to observe this hemispheric asymmetry in water vapor, and speculated that the underlying cause was differences in dynamics and diffusion. Water vapor decreases with height to very low values near the mesopause, so that descending air in the polar winter mesosphere causes seasonally low H_2O [*Orsolini et al.*, 2010]. The hemispheric difference in winter H_2O is therefore suggestive

of stronger winter descent in the NH than the SH. This difference is qualitatively consistent with the hemispheric differences in smoke volume density (Figure 5b), where more smoke in the NH winter compared to the SH is indicative of stronger transport in the NH. Note that SOFIE and WACCM agree on the hemispheric differences in winter H_2O (SH is ~10% > NH), but that the magnitude of the hemispheric differences in smoke are much larger in SOFIE (20 to 80%) than in WACCM (<10%) (Figure 5b). Nevertheless, it is too simplistic to infer a one-to-one correspondence between different tracer profiles and pure advective transport, as noted by *Ryan et al.* [2018]. Other factors such as chemistry or diffusion need to be considered [*Smith et al.*, 2011], and it is reasonable to assume that these would behave differently for smoke and H_2O. Differences in any one of these factors between WACCM and the observations could explain the differences in the smoke and H_2O hemispheric asymmetries.

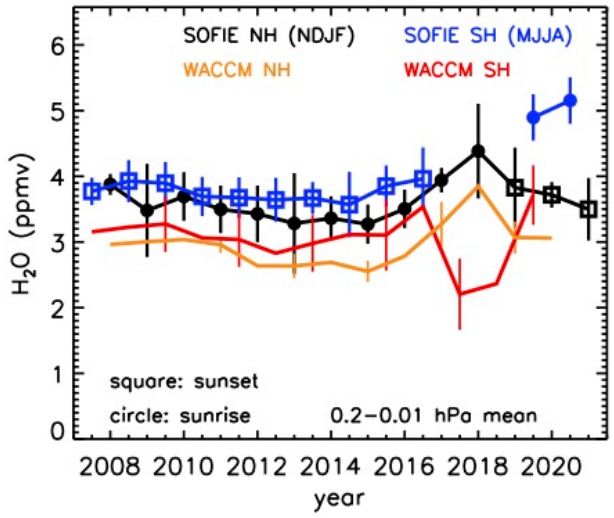

Figure 6. Time series of the winter mean water vapor from SOFIE and WACCM, as the average for 0.2 to 0.01 hPa. The results correspond to the latitudes in Figure 5a. Error bars indicate the standard deviation during each winter.

5. Meteoric Influx

Ablated meteoric influx (AMI) was derived through comparisons of SOFIE smoke volume density with WACCM runs conducted for different AMI values, as discussed in detail by *Hervig et al.* [2017a]. WACCM shows that when AMI is changed, smoke V changes by nearly the same

fractional amount at heights throughout the mesosphere. This is illustrated in Figures 7a - 7b, where the modeled V′ (average V for 0.2 - 0.01 hPa) is shown versus month and latitude from WACCM runs with different AMI. The approach determines AMI vs. V′ based on linear regression to the model results, AMI = $A + B$ V′, where A should be zero. WACCM results for AMI = 2, 8, and 11 t d^{-1} were used in the regressions (Figures 7a and 7b), with the additional constraint that the point (V′ = 0, AMI = 0) was included to encourage A to approach zero. Values of A have only small departures from zero (< 3%), which reflect the uncertainties in the approach (not shown). Because the SOFIE latitudes have changed over time (Figure 1), the regression to WACCM results was carried out for monthly zonal means over a complete range in latitude. Values of B at polar latitudes are found to change dramatically with season, with similar values during winter in both hemispheres (Figures 7c - 7d). High values of B in summer occur because smoke is depleted due to transport by the meridional circulation, while the regression was to the same annual global mean AMI values. The results are also found to vary with latitude (Figure 7d), where the variation is again driven by smoke transport. The uncertainties in derived MI are a combination of the SOFIE observational errors (~9% for monthly means), and the statistical uncertainty in the WACCM representation of V′ vs. AMI (~3% in polar winter). The AMI uncertainties (δAMI) are the root-sum-square of these terms, and the average δAMI for either hemisphere is ~10% during 2007 - 2021.

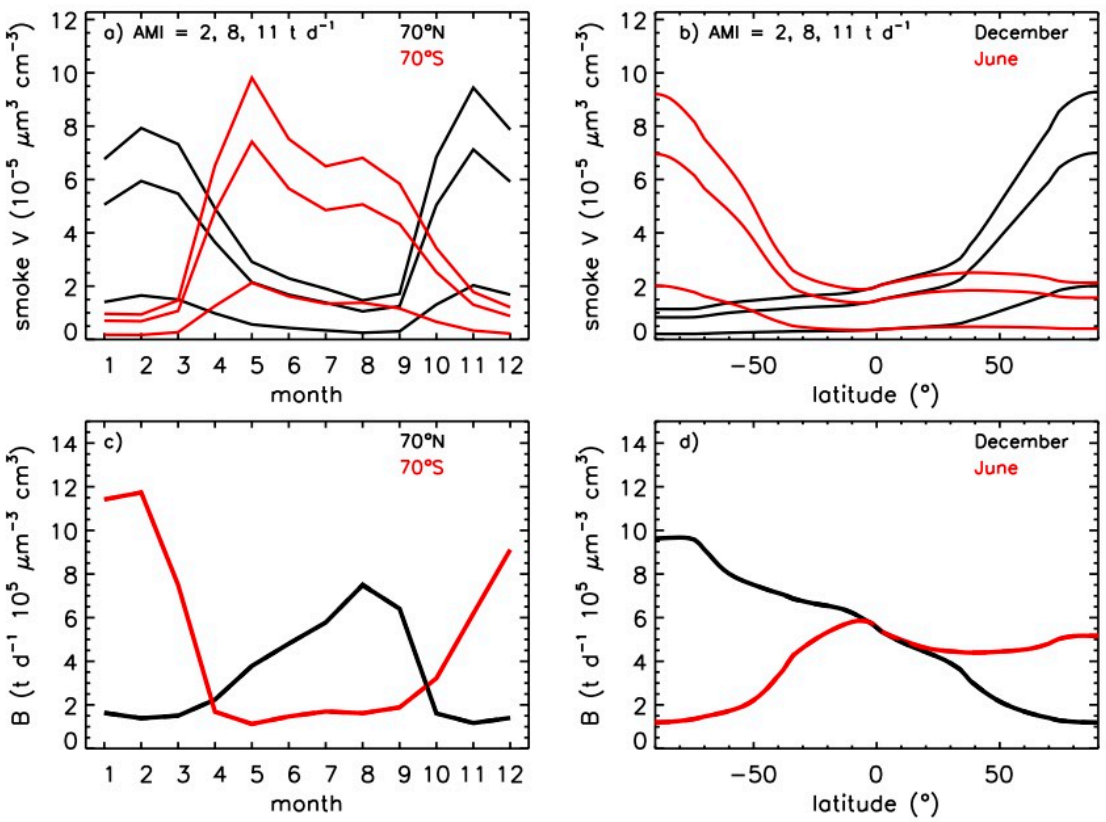

Figure 7. WACCM smoke volume density (V′, the 0.2 - 0.01 hPa average) as monthly zonal means from runs with meteoric influx of 2, 8, and 11 t d^{-1} (V′ increases with AMI). Results are shown a) versus month for 70°S and 70°N latitude, and b) versus latitude for December and June. The slope (*B*) for linear regression to WACCM AMI versus V′ is shown c) versus month at 70°S and 70°N, and d) versus latitude for December and June. *B* was determined from monthly zonal means for 2007 - 2015 (before the SOFIE orbit changed). Uncertainties in *B* during high latitude winter are ~3%.

Ablated influx is shown versus month in Figure 8 during autumn through spring when meteoric smoke is most abundant (e.g., Figure 4b). The AMI estimates have additional errors during the transitional months when the SOFIE - WACCM agreement is poorer (e.g., September in the NH, see Figure 4b), although this is not captured in the current uncertainty estimates. Recall also that SOFIE smoke observations are typically not obtained in high latitude summer due to

signal contamination by PMCs. The results in Figure 8 are for 2007 - 2017 when sunrise (sunset) was in the NH (SH). The average NH AMI is ~30% greater than for the SH, which is statistically significant in terms of the AMI uncertainties (~10%). If SOFIE and WACCM contained the exact same seasonal variation in mesospheric smoke, however, then the AMI derived here should be constant throughout the year (by definition). Thus, the monthly variations in AMI can be interpreted as a byproduct of SOFIE - WACCM differences in the seasonal variation of smoke, as apparent in Figure 4b. The best AMI estimates from the SOFIE - WACCM comparisons will therefore be from multi-month averages, preferably during winter when smoke is elevated and relatively stable in time.

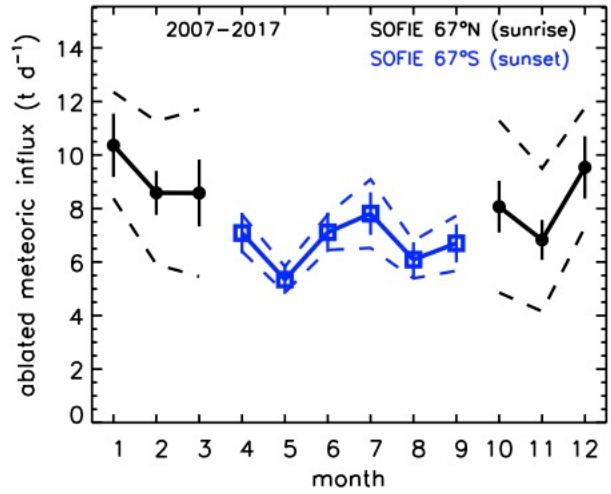

Figure 8. Ablated meteoric influx as monthly averages of SOFIE results during 2007 - 2017 when sunrise (sunset) was near 67°N (67°S). Vertical bars indicate the AMI uncertainty (δAMI, see text). Dashed lines indicate the standard deviation for the included years.

Ablated meteoric influx during 2007 - 2021 is shown as winter averages in both hemispheres in Figure 9, where the results are mostly for polar latitudes. AMI in the NH is typically greater than in the SH, with averages during 2007 - 2021 of 8.4 ± 2.0 t d^{-1} in the NH, and 6.2 ± 1.4 t d^{-1} in the SH (± standard deviation of 14 years). For both hemispheres combined AMI is 7.3 ± 2.0 t d^{-1}. The above standard deviations for 2007 - 2021 are ~22%, while the AMI uncertainty based on SOFIE and WACCM errors combined is ~10%, for either hemisphere. The results

indicate inter-annual variations in meteoric influx that are often statistically significant. Other observation of meteoric influx have shown year-to-year variability, including radars [e.g., *Janches et al.*, 2004] and satellite instruments [*Malaspina et al.*, 2016]. It is thus possible that the SOFIE inter-annual variations indicate real variability in meteoric influx, but this will be the topic of future studies.

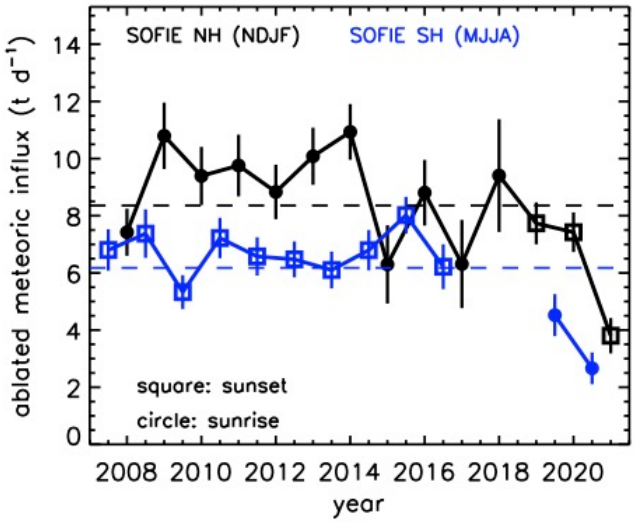

Figure 9. Time series of SOFIE AMI as winter means in the NH (November - February) and SH (May - August). The results correspond to latitudes as in Figure 5a. Note that sunrise (circle) and sunset (square) latitudes switched hemispheres in ~2018. The average AMI in the NH (8.4 t d^{-1}) and SH (6.2 t d^{-1}) are indicated by dashed lines. Error bars indicate the standard deviation for the included months.

The AMI derived here from the SOFIE-WACCM comparisons were anticipated to be equal in both hemispheres, yet hemispheric differences (NH > SH) exist during most years (Figure 9). This is due in part to hemispheric differences in SOFIE smoke volume density, that are weaker in WACCM (Figure 5b). Indeed, if WACCM had the same hemispheric differences in smoke V′ as SOFIE, then the resulting AMI would be equal in both hemispheres. Biases between the SOFIE sunrise and sunset observational modes were dismissed because the hemispheric difference persists after 2018 when sunrise switched from the NH to SH (see Section 4). Transport in the model was dismissed because hemispheric differences in SOFIE and WACCM wintertime mesospheric H_2O are similar (Section 4). Another explanation could be a hemispheric asymmetry

in processes involving smoke microphysics (e.g., coagulation and sedimentation) and/or chemistry (e.g., depletion of gas phase Fe by something other than smoke) that is incomplete in WACCM. A final idea is suggested, which is that the hemispheric difference in SOFIE smoke is due to an asymmetry in meteoric influx that is not included in WACCM. *Malaspina et al.* [2016] report meteoric flux observations from the Wind satellite operating roughly 10^6 km from Earth, showing a seasonal variation in MI with a maximum in March and a minimum in September. This annual variation was traced to interstellar particles, which flow into the Earth's orbital direction in March. These observations are not considered in the *Fentzke, et al.* [2008] description of meteoric influx variations used in WACCM, and thus could be a component in the SOFIE - WACCM disagreement concerning the hemispheric differences in mesospheric smoke.

The final consideration is derivation of total meteoric influx (TMI) from the SOFIE ablated meteoric influx results. The present study treats meteoric smoke as Fe-rich olivine, which has an elemental abundance nearly identical to that of the ablated meteoric source (see Section 2). As a result, the conversion from AMI to TMI can be taken directly from the *Carrillo-Sánchez et al.* [2020] results, which give TMI / AMI = 28 ± 16 t d^{-1} / 8.3 ± 4.7 t d^{-1} = 3.4. The resulting TMI values from this work are 28.4 ± 6.8 t d^{-1} in the NH and 21.0 ± 4.9 t d^{-1} in the SH. For both hemispheres combined TMI is 25.0 ± 7.0 t d^{-1}. The stated uncertainties are the standard deviation of the winter values for 2007 - 2021 (e.g., Figure 9). Note that the uncertainty in the SOFIE TMI estimates reported above are the standard deviations over 14 years, and that the experimental errors represent an additional 10% uncertainty. It is furthermore arguable that the SOFIE TMI uncertainties could be increased due to propagation of the *Carrillo-Sánchez et al.* [2020] errors (~57%).

6. Summary

An improved SOFIE sunrise signal calibration has produced meteoric smoke extinction retrievals in the Northern Hemisphere, for the first time. The new observations are in good agreement with WACCM simulations concerning both the time and height dependence of smoke in the mesosphere. Comparing the SOFIE extinction measurements to WACCM requires knowledge of the smoke composition, to describe the optical properties that relate extinction to volume density. The present study assumes that smoke in the mesosphere exists purely as Fe-rich olivine with the justification that 1) it is detected optically by SOFIE, 2) it has the same elemental abundance of Fe, Mg and Si as predicted from meteoric ablation, and 3) it is anticipated by theory and laboratory experiments [*Saunders and Plane*, 2011]. With the assumption of olivine, SOFIE results indicate a global mean ablated meteoric influx of 7.3 ± 2.0 t d^{-1} (total influx of 25.0 ± 7.0 t d^{-1}), based on averages for both hemispheres during 2007 - 2021. The new SOFIE influx results agree with *Carrillo-Sánchez et al.* [2020] (within 11%) who used models and observations to derive an ablated influx of 8.3 ± 4.7 t d^{-1} (total influx of 28.0 ± 16 t d^{-1}). This closure provides further support for mesospheric smoke existing as olivine. Additionally, these new results reconcile previous differences between SOFIE influx estimates from *Hervig et al.* [2017a] (AMI = 3.3 t d^{-1}; TMI = 30 t d^{-1}) and *Carrillo-Sánchez et al.* [2016] (AMI = 7.9 t d^{-1}; TMI = 43 t d^{-1}).

Both SOFIE and WACCM show ~10% hemispheric differences in wintertime mesospheric H_2O (SH > NH), that are consistent with stronger transport in the NH winter vs. the SH. This difference in transport is also apparent in both the SOFIE and WACCM mesospheric smoke results, which show less smoke in the SH polar winter compared to NH winter. The open issue is that the hemispheric difference in smoke is greater in SOFIE (~36%) than in WACCM (~2%). Because the meteoric influx estimates rely on comparisons of SOFIE and WACCM, a hemispheric

difference emerges in the SOFIE influx values (~30%). While this difference is close to the combination of experimental uncertainties (~10%) and geophysical variability (~20%), it is persistent in time and bears some thought. Sunrise - sunset biases in the SOFIE observations were dismissed because the hemispheric difference persists after 2018 when sunrise switched from the NH to SH (vice versa for sunset). Transport in WACCM was dismissed because the hemispheric differences in H_2O are the same in WACCM and SOFIE. The parting ideas in this regard are incomplete chemistry or microphysics in the smoke simulations, or asymmetries in meteoric influx that are not represented in the model.

Acknowledgements. This work was funded in part by the AIM mission through NASA's Small Explorers Program under contract NAS5-03132. The modeling work at the University of Leeds was supported by the European Research Council (project number 291332 – CODITA). SOFIE data are available online at sofie.gats-inc.com. The updated SOFIE extinctions used in this study are available by contacting Mark Hervig (mark@gats-inc.com). The WACCM data sets generated for this work have been archived at the Leeds University PETAL (PetaByte Environmental Tape Archive and Library) https://petal.leeds.ac.uk/.

References

Bardeen, C. G., O. B. Toon, E. J. Jensen, D. R. Marsh, and V. L. Harvey (2008), Numerical simulations of the three-dimensional distribution of meteoric dust in the mesosphere and upper stratosphere, *J. Geophys. Res., 113*, D17202, doi:10.1029/2007JD009515.

Bardeen, C. G., O. B. Toon, E. J. Jensen, M. E. Hervig, C. E. Randall, S. Benze, D. R. Marsh, and A. Merkel (2010), Numerical simulations of the three-dimensional distribution of polar mesospheric clouds and comparisons with Cloud Imaging and Particle Size (CIPS) experiment and the Solar Occultation For Ice Experiment (SOFIE) observations, *J. Geophys.*

356 *Res*., 115, D10204, doi:10.1029/2009JD012451.

357 Carrillo-Sánchez, J. D., D. Nesvorný, P. Pokorný, D. Janches, and J. M. C. Plane (2016), Sources
358 of cosmic dust in the Earth's atmosphere, *Geophys. Res. Lett., 43*,
359 doi:10.1002/2016GL071697.

360 Carrillo-Sánchez, J. D.; Gómez-Martín, J. C.; Bones, D. L.; Nesvorný, D.; Pokorný, P. Benna, M.;
361 Flynn, G. F.; Plane, J. M. C. (2020) Cosmic dust fluxes in the atmospheres of Earth, Mars,
362 and Venus, *Icarus*, *335*, art. no. 113395.

363 Feng, W., Marsh, D. R., Chipperfield, M. P., Janches, D., Hoffner, J. Yi, F., and Plane, J. M. C.
364 (2013): A global atmospheric model of meteoric iron, *Journal of Geophysical Research*, *118*,
365 9456–9474.

366 Fentzke, J.T., D. Janches, and J.J. Sparks (2008), Latitudinal and seasonal variability of the
367 micrometeor input function: A study using model predictions and observations from Arecibo
368 and PFISR, *J. Atmos. Solar-Terr. Phys*., doi:10.1016/j.jastp.2008.07.015.

369 Frankland, V. L.; James, A. D.; Feng. W.; Plane, J. M. C. (2015): The uptake of HNO_3 on meteoric
370 smoke analogues, *Journal of Atmospheric and Solar-Terrestrial Physics*, *127*, 150-160, *127*,
371 150-160, doi: 10.1016/j.jastp.2015.01.010.

372 Gardner, C. S., Alan Z. Liu, D. R. Marsh, Wuhu Feng and J. M. C. Plane (2014), Inferring the
373 Global Cosmic Dust Influx to the Earth's Atmosphere from Lidar Observations of the Vertical
374 Flux of Mesospheric Na, *J. Geophys. Res. Space Physics*, DOI: 10.1002/2014JA020383.

375 Gordley, L. L., et al. (2009), The Solar Occultation For Ice Experiment (SOFIE), *J. Atmos. Sol.-*
376 *Terr. Phys*., *71*, 300-315, doi:10.1016/j.jastp.2008.07.012.

377 Gelaro, R., McCarty, W., Suárez, M. J., Todling, R., Molod, A., Takacs, L., Randles, C. A.,
378 Darmenov, A., Bosilovich, M. G., Reichle, R., Wargan, K., Coy, L., Cullather, R., Draper, C.,

379 Akella, S., Buchard, V., Conaty, A., da Silva, A. M., Gu, W., Kim, G., Koster, R., Lucchesi,
380 R., Merkova, D., Nielsen, J. E., Partyka, G., Pawson, S., Putman, W., Rienecker, M., Schubert,
381 S. D., Sienkiewicz, M., & Zhao, B. (2017). The Modern-Era Retrospective Analysis for
382 Research and Applications, Version 2 (MERRA-2), Journal of Climate, 30(14), 5419-5454,
383 https://journals.ametsoc.org/view/journals/clim/30/14/jcli-d-16-0758.1.xml.
384 Hervig, M. E., L. L. Gordley, L. E. Deaver, D. E. Siskind, M. H. Stevens, J. M. Russell III, S. M.
385 Bailey, L. Megner, and C. G. Bardeen (2009), First satellite observations of meteoric smoke
386 in the middle atmosphere, *Geophys. Res. Letters*, doi:10.1029/2009GL039737.
387 Hervig, M. E., Brooke, J. S. A., Feng, W., Bardeen, C. G., Plane, J. M. C. (2017a), Constraints on
388 meteoric smoke composition and meteoric influx using SOFIE observations with models, *J.*
389 *Geophys. Res. Atmospheres, 122*, doi:10.1002/2017JD027657.
390 Hervig, M. E., C. G. Bardeen, D. E. Siskind, M. J. Mills, R. Stockwell, (2017b), Meteoric smoke
391 and H_2SO_4 aerosols in the upper stratosphere and mesosphere, *Geophys. Res. Letters, 44*,
392 doi:10.1002/2016GL072049.
393 James, A. D., D. R. Moon, W. Feng, P. S. J. Lakey, V. L. Frankland, D. E. Heard, J. M. C. Plane
394 (2017), The uptake of HO_2 on meteoric smoke analogues, *J. Geophys. Res.*, *122*, 554–565.
395 Janches, D., S. Palo, E. M. Lau, S. K. Avery, J. P. Avery. S. de la Peña, N. A. Makarov (2004),
396 Diurnal and seasonal variability of the meteor flux at the South Pole measured with radars,
397 *Geophys. Res. Lett., 31*, doi:10.1029/2004GL021104.
398 Lossow, S., J. Urban, H. Schmidt, D. R. Marsh, J. Gumbel, P. Eriksson, and D. Murtagh (2009),
399 Wintertime water vapor in the polar upper mesosphere and lower thermosphere: First satellite
400 observations by Odin submillimeter radiometer, J. Geophys. Res., 114, D10304,
401 doi:10.1029/2008JD011462.

402 Malaspina, D. M. and L. B. Wilson III (2016), A database of interplanetary and interstellar dust
403 detected by the Wind spacecraft, *J. Geophys. Res. Space Physics, 121*, 9369–9377,
404 doi:10.1002/2016JA023209.
405 Marsh, D. R., Janches, D., Feng, W. and Plane, J. M. C. (2013a): A global model of meteoric
406 sodium, *J. Geophysical Research*, *118*, 11,442–11,452.
407 Marsh, D. R., M. J. Mills, D. E. Kinnison, J. F. Lamarque, N. Calvo, and L. M. Polvani (2013b),
408 Climate Change from 1850 to 2005 Simulated in CESM1(WACCM), *J. Clim.*, *26*, 7372-7391.
409 Megner, L, D. E. Siskind, M. Rapp, and J. Gumbel (2008), Global and temporal distribution of
410 meteoric smoke; a 2D simulation study, *J. Geophys. Res., 113*, D03202,
411 doi:10.1029/2007JD009054.
412 Molod, A., Takacs, L., Suarez, M., and Bacmeister, J.: Development of the GEOS-5 atmospheric
413 general circulation model: evolution from MERRA to MERRA2, *Geosci. Model Dev., 8,*
414 1339–1356, https://doi.org/10.5194/gmd-8-1339-2015, 2015.
415 Orsolini, Y. J., Urban, J., Murtagh, D. P., Lossow, S., and Limpasuvan, V. (2010), Descent from
416 the polar mesosphere and anomalously high stratopause observed in 8 years of water vapor
417 and temperature satellite observations by the Odin Sub-Millimeter Radiometer, *J. Geophys.*
418 *Res., 115,* D12305, doi:10.1029/2009JD013501.
419 Plane, J. M. C. (2012), Cosmic dust in the earth's atmosphere, *Chem. Soc. Rev., 41*, 6507-6518,
420 doi: 10.1039/c2cs35132c.
421 Plane, J. M. C., W. Feng; Dawkins, E. C. M. (2015): The Mesosphere and Metals: Chemistry and
422 Changes, *Chemical Reviews*, *115*, 4497 - 4541, doi: 10.1021/cr500501m.
423 Russell, J. M. III, et al. (2009), Aeronomy of Ice in the Mesosphere (AIM): Overview and early
424 science results, *J. Atmos. Sol.-Terr. Phys.*, *71*, 289-299, doi:10.1016/j.jastp.2008.08.011.

Ryan, N. J., Kinnison, D. E., Garcia, R. R., Hoffmann, C. G., Palm, M., Raffalski, U., and Notholt, J. (2018): Assessing the ability to derive rates of polar middle-atmospheric descent using trace gas measurements from remote sensors, *Atmos. Chem. Phys., 18*, 1457–1474, https://doi.org/10.5194/acp-18-1457-2018.

Saunders, R.W. and J. M. Plane (2011), A photo-chemical method for the production of olivine nanoparticles as cosmic dust analogues, *Icarus, 212*, 373-382, ISSN 0019-1035, 10.1016/j.icarus.2010.12.019.

Schoeberl, M.R., and P.A. Newman (2015), Encyclopedia of Atmospheric Sciences (Second Edition), *Academic Press*, 2015, Pgs 12-17, ISBN 9780123822253, https://doi.org/10.1016/B978-0-12-382225-3.00228-0.

Smith, A. K., R. R. Garcia, D. R. Marsh, and J. H. Richter (2011), WACCM simulations of the mean circulation and trace species transport in the winter mesosphere, *J. Geophys. Res., 116*, D20115, doi:10.1029/2011JD016083.